Science of Sintering, **53** (2021) 445-459

https://doi.org/10.2298/SOS2104445T

UDK: 676.017.2; 692.533.1; 620.181.4

Cavitation Properties of Rendering Mortars with Micro Silica Addition

Anja Terzić[1*)], Marina Dojčinović[2], Ljiljana Miličić[1], Jovica Stojanović[3], Zagorka Radojević[1]

[1]Institute for Testing of Materials IMS, Vojvode Mišića Bl. 43, 11000 Belgrade, Serbia

[2]Faculty of Technology and Metallurgy, University of Belgrade, Karnegijeva 4, 11000 Belgrade, Serbia

[3]Institute for Technology of Nuclear and Other Mineral Raw Materials, Franchet d'Esperey 86, 11000 Belgrade, Serbia

Abstract:

Micro-silica is a highly efficient mineral additive whose role is reflected in improvements of microstructure packing, strength and durability of non-shaped composite building materials such as concrete and mortar. A comparative study of performances of rendering mortars with different quantities of micro silica was conducted. The experimental program included production of reference mortar based on Portland cement and quartz sand (CM) and three mortars with 5, 10, and 15 % addition of micro silica (SCM-5, SCM-10, and SCM-15). The effect that micro silica addition has on the thermal behavior and mechanical properties of mortars was discussed. Hydration mechanisms and thermally induced reactions were studied at temperatures ranging from ambient to 1100 °C by differential thermal analysis. The results were supported by X-ray diffraction analysis. The cementing efficiency of micro silica was assessed by cavitation erosion test. The changes in the morphology of mortar samples prior and upon cavitation testing were monitored by means of the scanning electron microscope imagining. It was found that 5 % of superfine micro silica (SCM-5 mortar) has positive effects on mechanical strengths (15 % increase in compressive strength) due to microstructure densification arising from the successive filling of voids by the micro silica. Addition of micro silica also improved the cavitation erosion resistance in comparison with reference cement mortar (SCM-5 showed cavitation velocity as low as 0.09 mg/min). This qualifies mortars with micro silica addition as building materials which can be safely employed in potential hydro-demolition environment.

Keywords*: Construction materials; Micro-filler; Composites; Thermal analysis; Mechanical properties.*

1. Introduction

Non-shaped cement based construction products such as concrete, including refractory concrete, and mortar were the most consumed materials on the planet during 20th century. Since these are artificial building materials designed for various types of construction works, this trend and their usage rate will remain unchanged in this century as well. Regardless of the binder being Portland cement or calcium aluminate cement, it is

*) **Corresponding author:** anja.terzic@institutims.rs

manufactured using natural resources which eventually will lead to their depletion. Cement factories produce large amount of carbon dioxide, which categorizes them as one of the main contributors to the greenhouse effect. In order to alleviate this problem the world-wide scientific society is on the quest to find adequate material which can be used as cement replacement or at least partial cement replacement. While this alternative raw material has to have positive effect on the strength and durability of the concrete/mortar, it is preferable that this resource is of secondary nature (a waste or by-product) or at least economically sustainable primary raw material. So far various pozzolanic materials which can be used as cement replacement have been identified: fly ash, bottom ash, clayey materials, metakaolin, ground granulated blast furnace slag, municipal waste ash, rice husk ash, silica fume, etc [1-5]. Silicon dioxide products (silica fume, micro silica, nano silica, colloidal silica, etc.) are in focus of recent researches because, besides good mechanical performances, these mineral additives contribute to the resistance and durability of a building material: high temperatures, acid attack, sea-water, sewage, effluents from the industries, and high mineral contained water [6-8].

Durability of concrete is an important concern for construction professionals as well as constant subject of on-going investigations. Numerous researchers confirmed positive influence of micro silica addition on the performances of this type building material. For instance, the combination of metakaolin and micro silica made significant impact on the strength characteristics of self-compacting concrete (SCC). Precisely, SCC concrete with 10 % replacing of cement with superfine silica resulted in 24.5 % increasing strength after 7 days and 38.9 % increasing strength after 28 days [9]. Addition of micro silica and sugarcane bagasse ash improved concrete's resistance to sulphate and chloride attack. Registered weight loss for the blended concrete immersed in H_2SO_4 was 6.25 % after 56 days and 10.28 % after 90 days. The concrete immersed in HCl showed the weight loss of 3.7 % and 7.2 % after 56 days and 90 days, respectively [10]. It was found that the addition of micro silica (10 %) and ground granulated blast furnace slag (30 %) might be considered as an optimum mix for 28-days strength to produce economical ternary blended concrete [11]. Another study [12] found that the increase in silica fume content from 6 to 12 % influences the increase in compressive strength at all ages due to the development of dense microstructure and increase in hydration products. Rate of setting is faster in micro-silica concrete than in normal concrete due to rapid hydration of fine and reactive slilica particles. Bahrami et al. came to conclusion that by increasing the amount of micro silica, an enhancement in mechanical properties occurs, which is accompanied by a slight drop in rheological properties. Namely, micro silica increases the mix viscosity, but enhances the mechanical properties due to micro-filling effect and pozzolanic reactivity. In order to maintain the self-compacting characteristic it is suggested to limit the use of micro silica to 5 % [13]. Ghanei et al. found that micro silica as a cement replacement (10 %) improves the corrosion properties of reinforced concrete due to the micro-filler action and enhanced bonding capability of the SiO_2 particles [14]. With both nano silica and micro silica added together, concrete's carbonation resistance and water absorption as well as the microstructure are significantly more improved in comparison with concretes with only nano silica or micro silica added [15].

Cavitation is a wear which represents formation, growth, and collapse of steam or vapor gas bubbles in a flowing fluid [16,17]. Implosion of bubbles is caused by shock waves and micro-jet-stress concentrators whose energy is either dissipated within the liquid or absorbed by a solid contact surface. The impact formed by collapsing cavitation bubbles have amplitudes between the strength values on the boundary of large elongations and the tensile strength of the material, thus contributing to formation of elastic/plastic deformation and surface hardening. Impulse pressures with the amplitude larger than the tensile strength of the material cause damage and loss of the material mass, which is called cavitation erosion [16,17]. Various forms of cavitation have been investigated: cavitation effects on the structure

induced by the interaction between underwater blast and various boundaries [18], cavitation in thermoplastic-reinforced rubber composites upon cyclic testing [19], acoustic cavitation in the reservoir and effects on dynamic response of concrete dams [20], short-time cavitation (2 and 10 s) of concrete specimens [21], aggregate liberation from concrete by flow cavitation [22]. No studies could be found on the cavitation of concrete/mortar with silica addition.

In this paper, the performances of rendering mortars with different quantities of micro silica (0, 5, 10, and 15 %) were investigated. Hydration mechanisms and thermally induced reactions were studied by differential thermal analysis. The results were supported by X-ray diffraction analysis. The cementing efficiency of micro silica was assessed by cavitation erosion test. The changes in the morphology of mortar samples prior and upon cavitation testing were monitored by means of the scanning electron microscope imagining.

2. Materials and Experimental Procedures

2.1 Rendering mortars

Experimental rendering mortars were prepared from Portland cement (CEM I 42.5R Lafarge; specific surface area 292 m^2/kg; 97.5 % of particles less than or equal to 0.63 mm) and quartz sand (grain-size 0.063-4.0 mm; Mohs hardness 7; uncompacted bulk density 1640 kg/m^3 and compacted bulk density 1750 kg/m^3 according to grain size as base resources). Micro silica (Sidistar R 300, Elkem AS Materials) was used as mineral additive: specific surface area (BET) 20 m^2/g; median particle size 0.15 μm; coarse particles (325 mesh) less than 0.10 %; and density 2.2 g/cm^3. Micro silica is predominantly amorphous mineral additive as illustrated in Fig. 1.

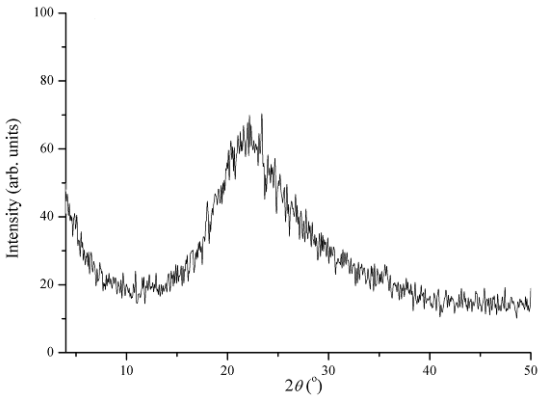

Fig. 1. XRD diffractogram of micro silica.

Micro silica was employed in 5, 10, and 15 % by mass of the binder. The mix design of the experimental mortars is provided in Table I. Chemical compositions of the employed raw materials and experimental mortars are presented in Table II. Chemical analyses were performed using EDXRF method (Spectro Xepos system).

Tab. I Mix design of experimental rendering mortars.

	CM	SCM-5	SCM-10	SCM-15
Cement (CEM I 42.5R)	25 %	23.75 %	22.5 %	21.25 %
Aggregate (quartz sand)	75 %	75 %	75 %	75 %
Micro silica	0 %	1.25 %	2.5 %	3.75 %
W/C ratio	0.5	0.51	0.54	0.57

Tab. II Chemical composition of raw materials and experimental mortars.

Oxide, %	SiO_2	CaO	MgO	Fe_2O_3	Al_2O_3	SO_3	Na_2O+K_2O	LoI*
CEM I 42.5R	19.28	59.57	2.55	2.93	6.39	1.73	1.56	1.5
Quartz sand	99.00	0.04	0.03	0.29	0.65	-	0.10	<0.03
Micro silica	96.62	0.350	0.108	0.103	0.227	-	1.77	0.82
CM	73.24	18.92	0.63	0.73	1.82	1.73	0.20	2.73
SCM-5	74.58	18.14	0.62	0.73	1.81	1.69	0.19	2.24
SCM-10	75.38	17.98	0.60	0.71	1.75	1.68	0.19	1.71
SCM-15	76.05	17.85	0.60	0.69	1.70	1.68	0.19	1.24

*at 1000°C

Mortar samples were prepared according to the standard procedure (SRPS EN 1015-2:2008) following the mix design provided in Table I. Cement, aggregate and micro silica were initially dry-homogenized using a laboratory mixer (Controls). The water was added later during mixing procedure. Fresh mortar was placed in steel moulds (40×40×160 mm) and kept in the storage chamber (95 ± 5 % relative humidity and 20°C (+3/-2 °C) temperature) for one day. Until a total of 7 days, demoulded samples were stored under the same conditions in the storage chamber. Afterwards, the samples were cured at 65 ± 5 % relative humidity for the following 21 days.

Rheology of the fresh mortar was determined via slump test using a flow table (SRPS EN 1015-3:2008). Determination of bulk density of fresh mortar and dry bulk density of hardened mortar was conducted according to SRPS EN 1015-6:2008 and SRPS EN 1015 - 10:2008, respectively. Determination of water absorption coefficient due to capillary action of hardened mortar was administered according to SRPS EN 1015-18:2008. Compressive strength was determined according to SRPS EN 1015 - 9:2008. Splitting tensile strength was obtained following the method provided in SRPS EN 1015-11:2008. Adhesive strength of hardened rendering mortar on substrate was tested according to SRPS EN 1015-12. All obtained testing results represent an average of minimum three specimens.

2.2 Instrumental methods applied

Mineral phase analysis of the pulverized hardened mortar samples was conducted using an automated Philips PW-1710 diffractometer with a Cu tube operated at 40 kV and 30 mA. The instrument is equipped with a diffracted beam curved graphite monochromator and a Xe-filled proportional counter. The diffraction data were collected in the 2θ Bragg angle range from 4 to 65^o, counting for 1 s (qualitative identification) at every 0.02 ^{o} step. The divergence and receiving slits were fixed 1 and 0.1, respectively. Measurements were performed at ambient temperature in a stationary sample holder.

Differential thermal analysis was conducted on a SETSYS TG-DTA/DSC apparatus (SETARAM Instrumentation) in the temperature range 20-1100 °C in an alumina pan at a constant heating rate of 10 °C/min and static air flow.

Fourier transform infrared analysis was performed using a Thermo Fisher Scientific Nicolet IS-50 spectrometer. Attenuated total reflectance technique was used for recording in range 4000-400 cm^{-1}, and 32 scans at resolution 4. Upon spectra recording, two corrections were performed: automatic correction of the base line and atmospheric suppression in order to eliminate signals obtained from gases (CO_2 and water vapor).

The morphology of hardened mortar samples was recorded via scanning electron microscope (TESCAN Mira3 XMU) at 5 kV. The samples were covered with Au-Pd alloy prior to imaging.

2.3 Cavitation resistance testing

Standard test method for cavitation erosion according to ASTM G32 -16 was employed on hardened mortar samples (a comprehensive description with apparatus scheme is provided in [22]). Due to the brittle nature of tested material, the ultrasonic vibratory cavitation method with a stationary sample was used. The sample holder was fixed at the bottom of the water bath. The mechanical vibratory concentrator was also submerged in water bath. Temperature of the water was maintained at 25±1 °C. The sample was positioned below the front surface of the vibratory concentrator separated by a 0.5 mm gap. The used frequency of mechanical vibrations was 20 kHz and the amplitude was 50 μm. A strong cavitation zone was formed underneath the front surface of the concentrator and the stationary-tested sample. The water from the water bath was cooling the sample in order to maintain its temperature constant. A continuous water flow created a pressure field stimulating the implosion of cavitation bubbles on the mortar sample surface.

Mass loss of each investigated sample and cavitation testing times were registered. The test output represents an average of minimum three testing per mortar (i.e. CM, SCM-5, SCM-10, and SCM-15). Cavitation rate of mortar was calculated as the total mass loss of the sample after the total testing time [23]. The cavitation testing periods were: 15, 30, 60, and 120 min. Upon each testing the samples were dried and the mass loss was measured with an analytic accuracy of ± 0.1 mg.

3. Results and discussion

3.1 Characterization of mortars with micro silica addition

Qualitative analysis of the mineral phase composition of CM, SCM-5, SCM-10, and SCM-15 mortars, conducted upon samples' curing for 28 days, are presented in Fig. 2. At this point all hydration reactions have been completed, final mineral phase composition is established, and all mortars achieved at least 95 % of their final mechanical strengths. The positions of the main XRD reflections and their intensities (in arbitrary units – *au*) are summarized in Table III.

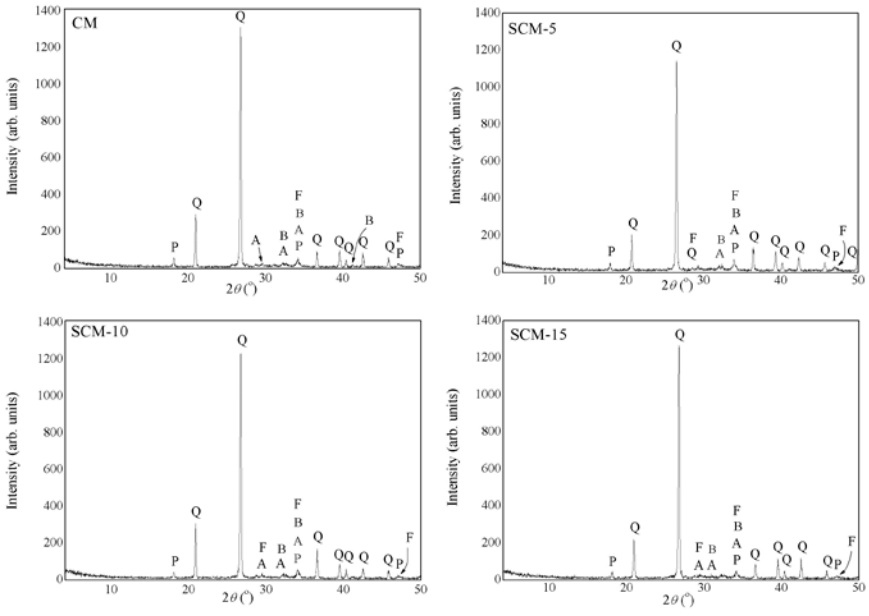

Fig. 2. XRD diffractograms of CM, SCM-5, SCM-10, and SCM-15 mortars.

The crystalline structure of cement mortar (CM) determined using X-ray diffraction analysis (Fig. 2) showed the common combination of cement minerals, which are the outcome of the cement hydration and subsequent hardening. The identified major and minor single or multiple phases are: C_3S (Alite – A in Fig. 2, Ca_3SiO_5, JCPDS-49-0442•), β-C_2S – (Belite – B in Fig. 2, β-Ca_2SiO_4, JCPDS-49-1673), $C_4(A,F)$ - (Brownmillerite – F in Fig. 2, Ca_2FeAlO_5, JCPDS-71-0667), P - (Portlandite, $Ca(OH)_2$, JCPDS-72-0156), and Q - (quartz, SiO_2, JCPDS-46-1045). Despite the crystallinity of the investigated sample being rather poor, alite and belite are the most abundant phases, as they are products of hydration process and chemical reactions between the main oxides in cement (CaO and SiO_2). Calcium hydroxide in crystalline form of Portlandite was also detected in the investigated cement mortar sample. Brownmillerite is a less abundant phase due to the small quantity of iron (III) oxide (2.93 %) in cement. The majority of XRD reflections are positioned between 20° and 50° in XRD diffractogram. Two prominent reflections (at 21° and 27°) correspond to quartz. Intensities of the observed reflections are 200 and 1300 arbitrary units. This highly crystalline mineral phase corresponds to SiO_2 from aggregate, i.e. quartz sand, which is not a reactive component in the mortar mix. Cement mineral phases are located between 29° and 50° mainly as groups of overlapped reflections. The addition of predominantly amorphous micro-silica to mortar mix-design (SCM-5, SCM-10, and SCM-15) did not cause major changes in XRD reflection patterns and their intensities as it can be seen in Fig. 2.

Tab. III Positions and intensities of main XRD reflections.

Mineral	Q				P		C_3S	βC_2S	$C_4(A,F)$
Location	21°	27°	37°	40-45°	18°	34°	30-50°	30-50°	30-50°
	Intensity (in arbitrary units)								
CM	300	1300	100	100	25	25	10	10	10
SCM-5	200	1190	120	120	25	25 u	10	10	10
SCM-10	310	1250	190	90	25	10 u	10	10	10
SCM-15	220	1280	80	100	25	10 u	10	10	10

Fig. 3 presents the infrared spectra of experimental mortars CM, SCM-5, SCM-10, and SCM-15 recorded after 28 days of curing, with the spectrum ranging from 400 to 4000 cm^{-1}. The wave numbers associated to the characteristic IR bands are summarized in Table IV.

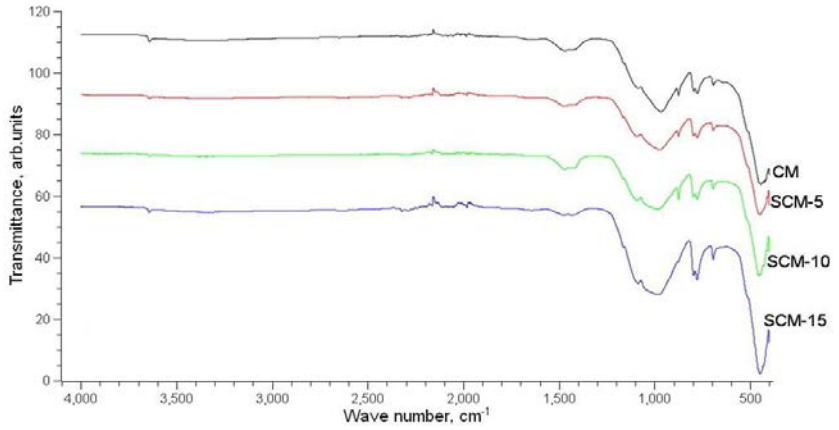

Fig. 3. FTIR spectra of experimental mortars.

•Powder Diffraction File/Cards. Joint Committee on Powder Diffraction Standards (JCPDS), Swarthmore, PA.

Tab. IV Position of infrared bands in attenuated total reflection FTIR spectroscopy of mortars.

IR band	1	2	3	4	5	6	7	8
	Wave number, cm^{-1}							
CM	444.03	693.77	776.25	865.53	964.37	1101.25	1468.0	3641.49
SCM-5	444.04	694.07	778.57	872.44	971.08	1120.05	1472.89	3642.25
SCM-10	444.57	694.26	779.67	874.57	976.23	1127.29	1479.52	3643.04
SCM-15	444.52	694.26	779.18	879.45	984.49	1131.24	1485.43	3644.45

Complex chemical and mineralogical compositions of the investigated rendering mortars with micro silica addition instigated equally complex spectral relationships between the groups present in FTIR spectra. Besides the single effect at approximately 3640 cm^{-1}, three main regions can be observed in the FTIR spectra: 1000-1600 cm^{-1}, 600-1000 cm^{-1}, and 400-600 cm^{-1}.

A unique peak was registered in CM, SCM-5, SCM-10, and SCM-15 positioned at 3641.49, 3644.25, 3643.04, and 3642.45 cm^{-1}, respectively. This effect most likely corresponds to O-H bond. Namely, the water bands (H_2O) are usually correlated with the peaks in the 3500 – 3700 cm^{-1} region. These peaks are caused by the υ3 vibration of water in cementitious materials [24-26]. The recorded band at approximately 3640 cm^{-1} also highlights the presence of mineral portlandite [27], which was detected by XRD analysis. The peaks present in SCM-5, SCM-10 and SCM-15 mortars are slightly shifted to higher wave numbers (Table IV) which can be explained as an effect of micro silica addition.

The peaks in the 1000-1600 cm^{-1} region can be associated with the carbonate bonds. The peaks detected at 1468.0, 1472.89, 1479.52, and 1485.43 cm^{-1} correspond to C–O bond, i.e. precisely to the asymmetric stretching of CO_3^{2-} [28]. Micro silica addition caused shifting of the corresponding peaks to a higher wave number. The effects occurring between 1400 cm^{-1} and 1600 cm^{-1} can be related to Ca-O bond. This is in agreement with the results of XRF and XRD analyses which identified high percentage of CaO and calcium based cement minerals. Assumption is that effects occurring in this sequence of the FTIR spectra are caused by the hydration process and the bending υ2 vibration of irregularly bound water [24-26]. Also, C-O bond which shows strong bands at 1363 cm^{-1} and 1364 cm^{-1} is correlated to monocarbo-aluminate and hemicarbo-aluminate [27]. Si-O bond with strong intensity of the band at 1115 cm^{-1} is correlated to the formation of ettringite. CM, SCM-5, SCM-10 and SCM-15 samples exhibited mentioned bands at 1101.25, 1120.05, 1127.29, and 1131.24 cm^{-1}, respectively. Again, the presence of micro silica in the mortar samples led to shifting of the corresponding peaks to a higher wave number. Regarding 1000-1600 cm^{-1} region, it is extremely difficult to distinguish single bands due to the complex cement chemistry and superposing of the effects in one huge bump on the FTIR diagram.

The peaks in the 600-1000 cm^{-1} are mostly Al-O and Si-O related. Si-O band corresponds to the most prominent effects. The effect at approximately 960-971 cm^{-1} corresponds to strong Si–O–Si asymmetrical stretching vibration [27]. For standard cement mortar this peak is positioned at 964.37 cm^{-1}. Mortars with 5, 10, and 15 % of micro silica addition have their peaks shifted to a higher wave number. Peaks at 860 cm^{-1} and 780 cm^{-1} correspond to medium intensity Si-O bond. Effect at 690 cm^{-1} corresponds to low intensity Si-O band (out of plane vibration). Al-O bond with low intensity band at 857 cm^{-1} corresponds to ettringite. Another medium intensity band located at 954 cm^{-1} corresponds to monocarbo-aluminate [27]. Main C-S-H peaks are located in the range between 900-1100 cm^{-1} which marks the formation of colloidal gel like structure [27]. As it can be seen from Tab IV the effects marked with 3, 4 and 5 were shifting to a higher wave number with increasing percentage of micro silica addition

The peaks in the 400-600 cm^{-1} mostly correspond to Si-O bonds. Namely, the effects located at 450 cm^{-1} are related to strong intensity Si-O bands (in plane vibrations) [27]. Also, several additional small Si-O bands located in vicinity of 500 cm^{-1} were registered in mortar samples. The Si-O in FTIR spectra is assumed to reflect the dissolution of alite and the polymerization of silica to form calcium silicate hydrate C-S-H [24-26].

Thermal behavior and hydration mechanisms of CM, SCM-5, SCM-10 and SCM-15 mortars were monitored via differential thermal analysis. The obtained curves are presented Fig. 4.

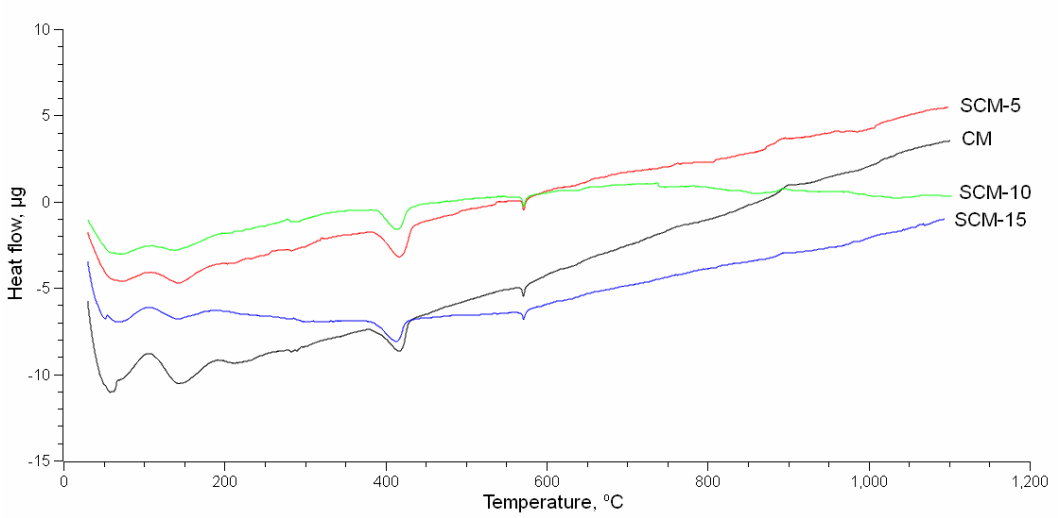

Fig. 4. DTA diagrams of experimental mortars.

The first significant endothermic effect can be seen at 75.0°, 75.3°, 85.6°, and 90.2°C for CM, SCM-5, SCM-10, and SCM-15 mortars, respectively. The initial effect is usually related to loss of chemically-non-bonded (free) water. This effect is more pronounced for cement mortar (CM). Mortars with micro silica addition showed less intense initial reactions. An exothermic effect with maxima at 100.1, 100.5, 110.3, and 110.8 °C for CM, SCM-5, SCM-10, and SCM-15 mortars, respectively, followed. Cement mortar exhibited the most intense reaction. Finally, additional endothermic effects appeared at 150.0, 150.5, 155.1, and 155.6 °C for CM, SCM-5, SCM-10, and SCM-15 mortars, respectively. The initial effects are usually associated with the endothermic reactions such as dehydration of $AH_3 \cdot H_2O$ gel which takes place at approximately 120 °C, and the formation of ettringite and colloidal C-S-H gel (100-150 °C). The addition of micro silica caused shifting of the peak maxima towards slightly higher temperatures, i.e. decreased the rate of initial cement hydration.

The following significant effects appeared in the region from 400 to 600 °C. Namely, the maxima of the 410 °C endothermic peak were set very close: 412.6, 411.4, 410.3, and 410.0 °C for CM, SCM-5, SCM-10, and SCM-15 mortars, respectively. Similar disposition of maxima was registered for the following endothermic effect: 592.9, 591.7, 590.5, and 590.0 °C for CM, SCM-5, SCM-10, and SCM-15 mortars, respectively. The reactions which took place at these temperatures are usually associated with the decomposition of Portland cement's aluminate phase $C_{12}A_7$. The dehydration of the calcium aluminate and alumina hydrates is near completion at 500 °C. Also, the effects above 500 °C can also be partially caused by α- to β-quartz polymorphic transformation. The addition of micro silica accelerated hydration mechanism at later stages (400-600 °C interval). After the second group of endothermic effects, DTA curves proceeded into continuous and relatively smooth exothermic hump extending from 600 to 1100 °C. The hump comprised only a small

exothermic effect at approximately 900 °C, which appeared as a consequence of $CaCO_3$ calcination.

Experimentally determined physico-mechanical characteristics of fresh and hardened mortar samples including average values of mechanical strengths are provided in Tables V and VI.

As it can be seen from Tab. VI, the differences in initial mechanical strengths were less significant during early stages of mortar hardening. The differences in mechanical strengths significantly increased after 28 days. Namely, the compressive strength of SCM-5 measured after 28 days increased for 15 % in comparison with cement mortar (CM). Compressive strengths (28 days) of SCM-10 and SCM-15 were 19 and 36 % higher than that of CM. Similarly, micro silica induced the increase in 28-days-splitting tensile strength. TS-s of SCM-5, SCM-10 and SCM-15 were 11, 14, and 15 % higher than corresponding CM strength. Adhesive strengths of SCM-5, SCM-10, and SCM-15 were 12, 13, and 18 % higher than cement mortar adhesive strength.

Tab. V Physico-mechanical properties of experimental mortar samples.

	Workability, mm (fresh mortar)	Bulk density, kg/m^3 (fresh mortar)	Bulk density, kg/m^3 (hardened mortar)	Water absorption coefficient, $mg/m^2 \cdot min^{0.5}$
CM	187	2200	2140	0.518
SCM-5	183	2145	2081	0.508
SCM-10	183	2138	2070	0.505
SCM-15	181	2115	2056	0.503

Tab. VI Mechanical strengths of experimental mortar samples.

	CS*, MPa (2 d)	CS, MPa (7 d)	CS, MPa (28 d)	TS**, MPa (2 d)	TS, MPa (7 d)	TS, MPa (28 d)	AS***, MPa
CM	10.13	28.56	40.4	3.15	5.92	6.7	0.51
SCM-5	11.05	32.27	47.2	3.2	5.97	7.5	0.58
SCM-10	12.44	33.12	49.05	3.5	6.0	7.8	0.59
SCM-15	12.35	33.17	53.21	3.4	6.0	7.9	0.62

*CS - Compressive strength; **TS - Splitting tensile strength, ***AS - Adhesive strength of hardened mortar on substrate (concrete); d – days.

3.2 Cavitation resistance of mortars with micro silica addition

The display of the treated mortar samples CM, SCM-5, SCM-10, and SCM-15 upon cavitation resistance testing is illustrated in Fig. 5. The samples were exposed to cavitation erosion for 30, 60, 90, and 120 min. As it can be seen, all samples predominantly maintained their structural integrity. The visual examination of each sample led to conclusion that no visible major cracks were present. The mechanical strengths of the mortars were high enough to sustain the water pressure and therefore no breaking of the samples was recorded during projected testing intervals.

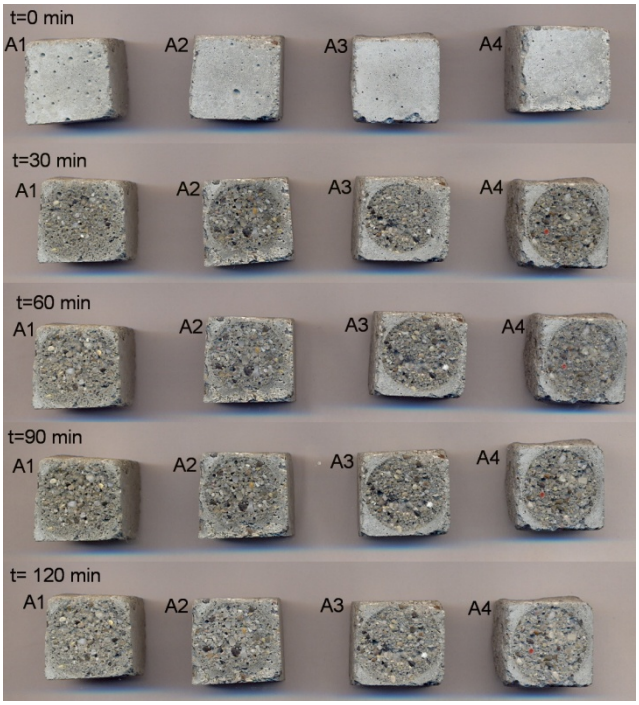

Fig. 5. Mortar samples (A1 = CM; A2 = SCM-5; A3 = SCM-10, and A4 = SCM-15) after 0, 30, 60, 90, and 120 min of cavitation erosion.

The cavitation erosion of the mortar samples CM, SCM-5, SCM-10, and SCM-15 was numerically expressed as mass loss measured upon each testing period (30, 60, 60, and 120 min). The numeric values of mass loss and cavitation velocities are given in Table VII. Mass loss per testing sample in dependence of cavitation duration is illustrated as a histogram in Fig. 6(a). Three samples were used for each series of tested samples and the results represent the mean value of these measurements for each test interval. This is a quantitative measurement of the intensity of destruction of materials under the action of cavitation. Cavitation velocities per testing mortar type are presented in Fig. 6(b). According to the ASTM G32 standard, the cavitation velocity is calculated as the total mass loss divided by the testing time [23]. Using the least squares method, the points of the diagram were approximated by a straight line whose slope tangent shows the loss of mass during the period of testing sequence, which represents the velocity of cavitation erosion. The point at which the linear curve intersects the abscissa shows the incubation period, i.e. the time that elapses before the occurrence of material damage [22]. Linear approximations of cavitation velocities per sample are as follows:

CM: $y = 0.4029 \cdot x - 0.262$ (1)

SCM-5: $y = 0.6973 \cdot x + 0.222$ (2)

SCM-10: $y = 0.17 \cdot x + 0.04$ (3)

SCM-15: $y = 0.0923 \cdot x + 0.058$ (4)

Tab. VII Mass loss of mortar samples after cavitation erosion.

	CM	**SCM-5**	**SCM-10**	**SCM-15**
Initial mass*, mg	2250	2230	2200	2190
Time, min	**Mass loss, mg/Cavitation velocity, mg/min**			
0	0/0	0/0	0/0	0/0
30	11.12/0.37	2.86/0.09	5.16/0.17	21.17/0.71
60	24.35/0.41	5.67/0.09	10.28/0.17	42.17/0.70
90	36.18/0.40	8.35/0.09	15.36/0.17	63.57/0.71
120	47.9/0.39	11.1/0.09	20.4/0.16	83.4/0.69
Avg. velocity, mg/min	0.39	0.09	0.17	0.70

*dimension of the testing sample: 10x10x10 mm

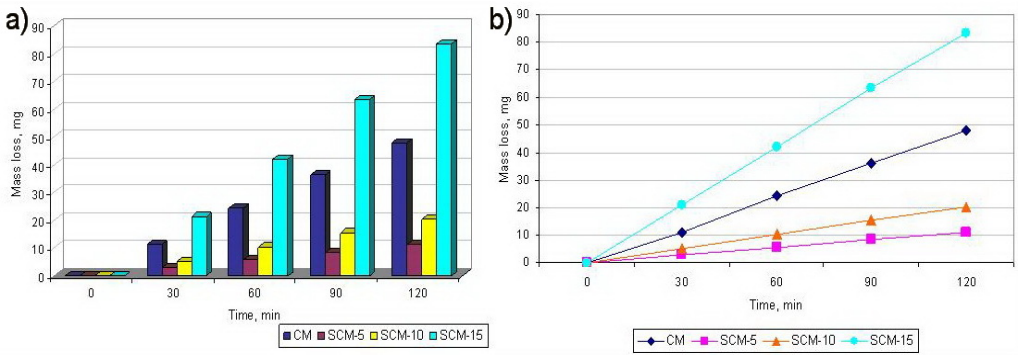

Fig. 6. (a) Mass loss and (b) cavitation erosion velocity of mortar samples after cavitation testing.

As it can be seen from Table VII and Fig. 6(a), cement mortar (CM) samples were significantly more prone to cavitation erosion in comparison with SCM-5 and SCM-10 mortars. Mass loss measured for CM sample per testing period was approximately 4 times higher than mass loss of corresponding SCM-5 sample, and 2.5 times higher than SCM-10 sample. Mortars with 15 % of micro silica addition showed the highest mass loss. Substandard values of mass loss of SCM-15 were 2 times higher than those of cement mortar. It can be concluded that micro silica addition in amounts up to 10 % improves microstructural packing and mechanical strengths due to more effective cementation, and thereby it contributes to cavitation erosion resistance. Application of micro silica in higher percentages (e.g. 15 %) leads to notable structural degradation during cavitation testing despite high mechanical strengths (Table VI).

Cement mortar exhibited higher average value of cavitation velocity (0.39 mg/min) than rest of experimental mortars. With only 0.09 mg/min, SCM-5 sample has the lowest cavitation erosion velocity among tested mortars. This means that relatively small percentage of micro silica addition (5 %) significantly contributed to the mortar mix design in terms of improved packing and cementation of heterogeneous mortar structure. SCM-10 also showed relatively low average value of cavitation erosion (0.17 mg/min). Anticipated degradation of SCM-5 and SCM-10 mortars in contact with water and air bubbles will be slower and significantly less damaging than degradation of standard cement mortar. SCM-15 exhibited inadequate resistance to cavitation erosion by having two times higher velocity (0.7 mg/min) than cement mortar.

If the degradation throughout the course of time was compared, CM exhibited slow degradation (small mass loss, slow velocity) during the first quarter of examination, i.e. initial

30 min. The cavitation erosion parameters increased during the second quarter. During last two quarters cavitation erosion slowed down its rate. SCM-5 showed constant cavitation erosion velocity and mass loss during entire period of 120 min. SCM-10 exhibited constant cavitation erosion velocity from first to third quarter, while during fourth quarter velocity slightly decreased. SCM-15 showed small variations in cavitation erosion velocities, i.e. velocities were higher during 1st and 3rd quarter and slower during the final quarter of testing.

The morphology of the superficial damage on the mortar samples due to the cavitation erosion was analyzed by scanning electron microscopy (Fig. 7). Based on the previous analysis and interpretation of the behavior of mortar samples during the time of exposure to cavitation, their stability and resistance were correlated the structure and mechanical properties of the material.

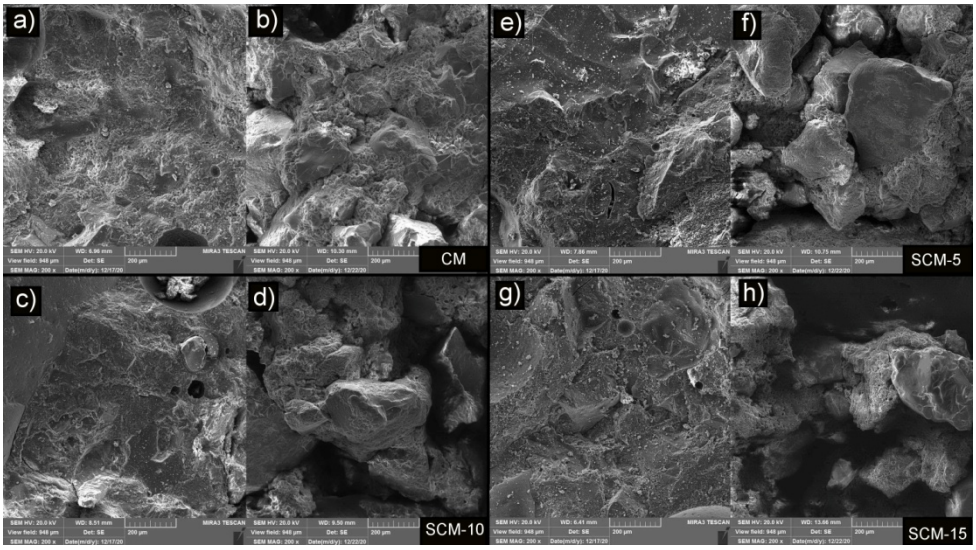

Fig. 7. SEM microphotographs of CM, SCM-5, SCM-10, and SCM-15 mortars before cavitation and after 120 min of cavitation erosion.

The morphology of cement mortar sample prior to cavitation is visualized in Fig 7(a). The microphotograph shows a compact well-cemented structure where comparatively bigger aggregate grains are covered with cement particles of micron sizes. As mortar is by definition a porous material, the image depicts multitude of micro- and nano-sized pores and voids. Wider pits and missing grains are consequence of the damages occurred during crushing of the sample prior to SEM imagining and they are excluded from examination. Fig. 7(b) represents morphology of a cement mortar sample after total of 120 min of cavitation erosion testing. The sample lost approximately 2.1 % of its mass (Table VII). The lost material constitutes primarily of cement particles. Quartz grains are clearly visible in this image. Quartz aggregate has significantly higher hardness which makes it prone to cavitation erosion. The cement-aggregate transition zone is also a weak spot for hydro-demolition processes. Larger pits and pores visible in Fig. 7(b) have opened due to the action of the air bubbles during cavitation erosion.

Sample SCM-5 (Fig.7(e)) had lower starting porosity and improved structural packing due to the application of mineral additive in its mix design. Cavitation led to the loss of bonding material, i.e. cement and micro silica particles. However, only 0.5 % of initial sample mass was lost during the cavitation testing. As it can be seen in Fig. 7(f), quartz grains are still surrounded with a thick ring of solid cementitious binder which means that the cement-aggregate transition zone has not suffered major degradation. This outcome will have

a positive influence on mortar's mechanical properties upon cavitation. Despite having low starting porosities both sample SCM-10 (Fig. 7(c)) and SCM-15 (Fig. 7(g)) exhibited low cavitation resistance. Namely, cavitation testing let to a high extent of degradation as it can be seen in Fig. 7(d) and Fig. 7(h) for samples SCM-10 and SCM-15, respectively. SCM-10 lost 1 % of its initial mass, while SCM-15 suffered the biggest mass loss (3.8 %). Transition zone is weakened by cavitation erosion and large percentage of quartz grains remained without its cementing material which will unmistakably lead to the degradation of mechanical characteristics and performances of these mortars upon hydro-demolition.

4. Conclusion

Ultrasonic vibratory method for determination of effects of the cavitation erosion was applied for the first time on the cement mortars with addition of micro silica. The performances of experimentally obtained rendering mortars were assessed using several instrumental methods and standard laboratory testing. The cavitation properties of mortars were obtained using standard ASTM G32-92 method and scanning electron microscopy. The main conclusions are summarized below:

- Addition of up to 15 % of micro-silica to mortar mix-design did not cause significant changes in X-ray diffraction patterns, i.e. no mineralogical alternations occurred.
- Fourier transform infrared analysis recorded the shifting of present Si-O bands to positions in spectra with higher wave numbers due to the micro silica addition.
- Differential thermal peak maxima shifted towards higher temperatures (in 20-150 °C region) due to micro silica addition referring to a decrease in the rate of initial cement hydration. The addition of micro silica accelerated hydration mechanism at later stages (400-600 °C region).
- Differences in compressive, splitting tensile and adhesive strengths of CM, SCM-5, SCM-10 and SCM-15 were less significant during early stages of mortar hardening (up to 7 days). Mechanical strengths of mortars with different percentage of micro silica showed notable differences after 28 days.
- Cement mortars were more prone to cavitation erosion than SCM-5 and SCM-10 mortars. Higher percentage of micro silica (SCM-15) leads to notable structural degradation.

It was concluded that that 5 % of superfine micro silica (SCM-5 mortar) has positive effects on mechanical strengths (15 % increase in compressive strength) due to microstructure densification arising from the successive filling of voids by the micro silica. Addition of micro silica also improved the cavitation erosion resistance in comparison with reference cement mortar (SCM-5 showed cavitation velocity as low as 0.09 mg/min). This qualifies mortars with micro silica addition as building materials which can be safely employed in potential hydro-demolition environment.

Acknowledgments

This investigation is financially supported by Ministry of Education, Science and Technological Development of the Republic of Serbia (contract no.: 451-03-9/2021-14/ 200012).

The authors would like to express mutual gratitude to laboratories and colleagues from Institute of Technical Sciences SANU, Belgrade for recording DTA diagrams; Institute for Nuclear and other Mineral Raw Materials, Belgrade for recording FTIR spectra; and Faculty of Technology and Metallurgy of the University of Belgrade for recording SEM microphotographs; as well as prof. Zagorka Aćimović for constructive suggestions regarding cavitation procedure.

5. References

1. E. Felix, R. Carrazedo, E. Possan, Construction and Building Materials 266 (2021) 121050.
2. E. Moreno Bernal, M. Vlasova, P. Antonio Márquez, M. Kakazeyl, R. Guardian Tapia, Science of Sintering 52 (2020) 25.
3. P. Matos, J. Oliveir, T.Medina, D. Magalhães, et al., Construction and Building Materials 262 (2020) 120102.
4. W. Fahrenholtz, G. E. Hilmas Ruixing, Li Beihang, Science of Sintering 52 (2020) 1.
5. M. Rajasegar, C. Manoj Kumaar, Materials Today: Proceedings (2020) doi: 10.1016/j.matpr.2020.09.148.
6. G. Adil, J. Kevern, D. Mann, Construction and Building Materials 247 (2020) 118453.
7. D. Tripathi, R. Kumar, P. K. Mehta, A. Singh, Materials Today: Proceedings 27 (2020) 1001.
8. J. Bijeljić, N.Ristić, Z.Grdić, G. Topličić-Ćurčić, D. Đorđević, Science of Sintering 52 (2020) 231.
9. J. Seelapureddy, J. Bommisetty, M.V. Seshagiri Rao, Materials Today: Proceedings (2020). doi: 10.1016/j.matpr.2020.02.936
10. M. Ikramullah Khan, M. Sayyed, M. Meer Assad, Materials Today: Proceedings (2020). doi: 10.1016/j.matpr.2020.08.468
11. V. B. Reddy Suda, P. Srinivasa Rao, Materials Today: Proceedings 27 (2020) 805.
12. N. Bhalla, S. Sharma, S.Sharma, R. Siddique, Construction and Building Materials 162 (2018) 802.
13. N. Bahrami, M. Zohrabi, S. Ali Mahmoudy, M. Akbari, Journal of Building Engineering 31 (2020) 101361.
14. A. Ghanei, H. Eskandari-Naddaf, T. Ozbakkaloglu, A.Davoodi, Construction and Building Materials 262 (2020) 120768.
15. L. Gu Li, J. Ying Zheng, P. Ng, A. Kwan, Journal of Building Engineering 33 (2021) 101862.
16. A. Pola, L. Montesano, M. Tocci, G. M. La Vecchia, Materials 10 (2017) 256.
17. C. Feng, J. Shuyun, Applied Surface Science 16 (2014) 292, 16.
18. Z. Jin, C. Yin, Y. Chen, Y. D. Cui, B. C. Khoo, S. Jiao, H. Hua, Ocean Engineering 222 (2021) 108596.
19. C. E. Federico, G. Rauchs, O. Kotecky, S. Westermann, F. Addiego, Polymer 211 (2020) 123084.
20. F. Kalateh, R. Attarnejad, Finite Elements in Analysis and Design 47 (2011) 543.
21. A. W. Momber, Wear 241 (2000) 47.
22. A. W. Momber, International Journal of Mineral Processing 74 (2004) 177.
23. M. Dojčinović, Razaranje materijala pod dejstvom kavitacije, Monograph, Tehnološko-metalurški fakultet, Beograd (2013) ISBN: 978-86-7401-305-2.
24. Standard Method of Vibratory Cavitation Erosion Test, G32-92. Annual Book of ASTM Standards, Vol. 03.02. Philadelphia: ASTM; 1992.
25. S. Ghosh, S. Handoo, Cement and Concreat Research 10 (1980) 771.
26. A. Jose, M. R. Nivith, J. Murali Krishnan, R.G.Robinson, Construction and Building Materials 263 (2020) 120136.
27. K. Kupwade-Patil, S. Palkovic, A. Bumajdad, C. Soriano, O. Büyüköztürk, Construction and Building Materials 158 (2018) 574.
28. M. Horgnies, J. J. Chen, C. Bouillon, WIT Transactions on Engineering Sciences 77 (2013) 251.
29. S. Kumar Das, S. Mohammed Mustakim, A. Adesina , J. Mishra, et. al., Journal of Building Engineering 32 (2020) 101780.

Сажетак: *Микро силика је високо ефикасан минерални додатак чија се улога огледа у побољшању паковања честица унутар микроструктуре, повећању чврстоће и трајности необликованих композитних грађевинских материјала као што су бетон и малтер. Спроведено је упоредно истраживање перформанси конструктивних малтера са различитим количинама микро силике. Експериментални програм је подразумевао справљање референтног малтера на бази портланд цемента и кварцног песка (CM) и три малтера са додатком микро силике у количини 5, 10 и 15 % (SCM-5, SCM-10 i SCM-15). Праћен је утицај микро силика додатка на термичко понашање и механичка својства малтера. Механизми хидратације и термички индуковане реакције проучавани су диференцијалном термичком анализом на температурама у распону од амбијенталне до 1100 °C. Добијени резултати су даље разјашњени помоћу X-ray дифракционе анализе. Везивна ефикасност микро силике процењена је тестом кавитационе ерозије. Промене у морфологији узорака малтера пре и после испитивања кавитације праћене су помоћу скенирајућег електронског микроскопа. Утврђено је да 5 % суперфиног микро силика додатка (малтер SCM-5) има позитивне ефекте на механичке чврсто ће (повећање притисне чврстоће од 15 %) што је последица дензификације микроструктуре настале услед попуњавања празнина честицама микро силике. Додавањем микро силике побољшана је и кавитациона отпорност у поређењу са референтним цементним малтером (SCM-5 је имао брзину кавитације од само 0,09 mg/min). Све претходно наведено квалификује испитиване малтере са додатком микро силике као грађевинске материјале који се могу безбедно користити у потенцијалном хидро-деструктивном окружењу.*

Кључне речи*: грађевински материјали, микро пунило, композити, термичка анализа, механичка својства.*